

Slab-Specific Projection-Resolved Optical Coherence Tomography Angiography for Enhancing En Face Polyp Detection in Polypoidal Choroidal Vasculopathy

Nida Wongchaisuwat,^{1,2} Jie Wang,² Tristan T. Hormel,² Yali Jia,² Elizabeth S. White,² Nuttawut Rodanant,¹ and Nopasak Phasukkijwatana¹

¹Department of Ophthalmology, Faculty of Medicine Siriraj Hospital, Mahidol University, Bangkok, Thailand

²Casey Eye Institute, Oregon Health & Science University, Portland, Oregon, United States

Correspondence: Nopasak Phasukkijwatana, Department of Ophthalmology, Faculty of Medicine Siriraj Hospital, Mahidol University, 2 Wanglang Rd., Bangkoknoi, Bangkok 10700, Thailand;
nopasak.sioph@gmail.com.

Received: April 4, 2024

Accepted: December 4, 2024

Published: January 6, 2025

Citation: Wongchaisuwat N, Wang J, Hormel TT, et al. Slab-specific projection-resolved optical coherence tomography angiography for enhancing en face polyp detection in polypoidal choroidal vasculopathy. *Invest Ophthalmol Vis Sci.* 2025;66(1):9. <https://doi.org/10.1167/iovs.66.1.9>

PURPOSE. A projection-resolved optical coherence tomography angiography (PR-OCTA) algorithm with slab-specific strategy was applied in polypoidal choroidal vasculopathy (PCV) to differentiate between polyp and branching vascular network (BVN) and improve polyp detection by en face OCTA.

METHODS. Twenty-nine participants diagnosed with PCV by indocyanine green angiography (ICGA) and 30 participants diagnosed with typical neovascular age-related macular degeneration (nAMD) were enrolled. Polyps were classified into three categories after using the slab-specific PR algorithm. Type 1 polyps were considered in high-elevated pigment epithelial detachment (PED) and displayed in green. Type 2 polyps were considered in low-elevated PED and encoded in yellow, similar to BVN structures. Type 3 polyps were not able to be detected on OCTA. The algorithms were tested in the nAMD group to differentiate PCV and typical nAMD.

RESULTS. With the algorithm, type 1 polyps were readily differentiated from BVN on en face OCTA. Polyp detection rate on en face OCTA only (type 1) was 68%, which was significantly improved from 30% when the algorithm was not used ($P = 0.0001$). To identify type 2 polyps, a combination of en face and cross-sectional OCTA images was needed and this resulted in a 91% polyp detection rate (types 1 and 2). The absence of luminal structure on OCT at the polyp site, small polyp size, and absence of halo on ICGA appeared to influence the polyp detection rate. When applying the algorithm to the nAMD group, 83% were correctly classified as typical nAMD (absence of type 1 polyps), whereas 17% showed false detection of polyps due to flow signals at the apices of large PEDs.

CONCLUSIONS. The slab-specific PR-OCTA with different color coding provides significant improvement in detecting polyp structures on en face OCTA, leading to rapid coronal visualization and diagnosis of PCV without the risk of dye injection.

Keywords: aneurysmal type 1 neovascularization (AT1), optical coherence tomography angiography (OCTA), slab-specific optical coherence tomography angiography (OCTA), slab-specific projection-resolved optical coherence tomography angiography (PR-OCTA), polyp detection

Polypoidal choroidal vasculopathy (PCV) is a type of choroidal neovascularization with distinctive morphologic characteristics. It is composed of a branching vascular network (BVN) with terminal aneurysmal dilatations called polyps. It is still controversial whether PCV is a distinct disease entity or is a variant of neovascular age-related macular degeneration (nAMD),¹ but it has been widely accepted as a subtype of nAMD.² PCV is much more common in Asian than in Caucasian populations, with prevalences of 20% to 78% and approximately 10% among patients with nAMD, respectively,^{3–5} and constitutes a major proportion of macular diseases in Asia. The prevalence is 78% in the Thai population with choroidal neovascularization.⁴

The current gold standard for diagnosis of PCV is indocyanine green angiography (ICGA), which involves intravenous injection of indocyanine green dye. However, this procedure can produce side effects, which vary from nausea to anaphylactic reaction to indocyanine green dye, and is available in only some ophthalmic centers.

Optical coherence tomography angiography (OCTA) allows depth-resolved visualization of retinal and choroidal vasculature without the use of dye.^{6–9} It detects signals arising from the motion of blood cells (flow) in tissue and highlights vessels against other static tissue components. OCTA procedures are noninvasive, simple, and fast enough (only a few seconds) to be easily repeated in every visit in order to monitor disease progression and response to treatments.



Several studies have explored the imaging capability of OCTA to detect PCV. It was found that OCTA was equal or superior to ICGA in the visualization of BVN.² However, the ability of OCTA to visualize polyps was limited, making the diagnosis of PCV by OCTA challenging.^{10–12} Several explanations were proposed, including slow and turbulent flow within the polyps and projection artifacts. Jia et al. used the split-spectrum amplitude-decorrelation angiography (SSADA) OCTA algorithm¹³ to detect PCV blood flow between each cross-sectional scan. They found faster flow velocity at the periphery compared to the center of polypoidal lesions.¹¹ In addition, Choi et al. and Rebhun et al. proposed the variable interscan time analysis (VISTA) OCTA-based algorithm for improving the detection sensitivity of PCV with slow flow.^{14,15} Different interscan times of 1.5 and 3 milliseconds were compared to detect relatively different blood flow speeds in polyps and BVN. Using this algorithm, 86% of polyps were detected, and they also found a higher flow speed in the periphery compared to the center of polyps.¹⁵ However, flow signals of polyps are often difficult to be distinguished from BVN just by observing en face OCTA alone. Segmentation slabs for en face visualization also play an important role in polyp detection, as the outer retinal slab could detect flow in polyps better than the choriocapillaris slab.¹¹ Moreover, segmentation can also be problematic as eyes with PCV usually have abnormal anatomy, such as pigment epithelial detachment (PED) and/or subretinal materials, which can make results from built-in automated segmentation algorithms spurious. Looking at the cross-sectional B-scan (axial view) with flow overlay may bypass the need for segmentation algorithms but requires more subjective judgment and expertise and may be time-consuming.¹⁶

Our study aims to improve polyp detection rate using en face OCTA alone by using our novel slab-specific projection-resolved optical coherence tomography angiography (PR-OCTA) algorithm to automatically distinguish polyp structures from adjacent BVN, resulting in polyps being labeled in green and BVN labeled in yellow on en face OCTA. This technique allows clinicians to easily visualize polyps leading to the rapid diagnosis of PCV by en face OCTA.

METHODS

The retrospective observational study includes patients with PCV at the Department of Ophthalmology, Faculty of Medicine Siriraj Hospital, Mahidol University, and typical patients with nAMD randomly selected from the OCTA data set at the Casey Eye Institute, Oregon Health & Science University, between November 2017 and October 2019. According to the tenets of the Declaration of Helsinki, the protocol was approved by the Institutional Review Board of Siriraj Hospital, Mahidol University (COA number Si 763/2019).

Patients at least 18 years of age diagnosed with PCV confirmed by ICGA (according to the EVEREST diagnostic criteria)¹⁷ with available OCTA images taken at the same period of ICGA were included. The study included both treated and treatment naïve patients at any stages (acute or chronic) and severity of the disease. Patients with significant ocular media opacity precluding adequate imaging and patients with other maculopathies that confounded the visualization of PCV lesions were excluded. OCTA images of typical patients with nAMD diagnosed by retinal experts were

included as a control group. OCTA images with a signal strength index of less than 60 were excluded from the study.

Demographic data, including age, sex, underlying diseases, duration, and treatment of PCV, were collected. Visual acuity (VA) and complete dilated ocular examinations were recorded. Fundus photography, fluorescein angiography (FA), ICGA, and OCTA images were reviewed. Two retinal specialists (authors N.P. and N.W.) independently made the diagnosis of PCV and an open adjudication resolved the disagreement between the two readers.

Simultaneous FA and ICGA were performed using a SPEC-TRALIS (Heidelberg Engineering, Heidelberg, Germany) or Optos confocal scanning laser ophthalmoscope (Optos, PLC, Dunfermline, Scotland). OCTA images (6 × 6-mm centered on the fovea) were obtained using the RTVue XR Avanti device (Optovue Inc., Fremont, CA, USA) with an A-scan rate of 70,000 scans/second, a light source of 840 nm and a bandwidth of 45 nm.

Polyp detection was aided by two image processing algorithms embedded in a custom COOL-ART (Center for Ophthalmic Optics & Lasers-Angiography Reading Toolkit) software developed by the authors using MATLAB (MathWorks, Natick, MA, USA). First, we used a guided bidirectional graph search method in order to generate retinal layer boundaries.¹⁸ The artificial intelligence (AI) correcting function embedded in our COOL-ART were utilized to correct the segmentation errors. Because polyps can cause large distortions in retinal structure this algorithm can sometimes fail; for this reason, we reviewed all scans and manually corrected any with segmentation errors. The average time to correct the segmentation errors was about 1 minute. Second, we used advanced projection artifact removal using a signal attenuation-compensated projection-resolved OCTA algorithm.^{19,20} This algorithm enhances the reflectance signals of capillaries in order to enhance in situ flow signals while removing projection artifacts. In tandem, these approaches helped to avoid the misidentification of polyp flow by preventing its removal in segmentation artifacts and avoiding ambiguity from projection artifacts.

Polypoidal lesions identified in OCTA are observed as a vascular flow in the posterior layer of the en face projection, located between RPE and Bruch's membrane. Typically, they appear as solid round structures or as close loop vessels at the distal termination of the branching vascular network. In cross-sectional OCT overlaid by OCTA, polyps typically appear as thick-walled luminal structures beneath peaked PEDs, with flow present inside the PEDs. Our study developed an auto-generated algorithm to highlight polyps by utilizing the thickness level of PED, distinguishing polyp structures from adjacent BVN. The algorithm considers high elevations of PEDs as polyps, which are displayed in a green signal. Conversely, low elevations of PED are encoded in yellow, representing BVN structures. The cutoff value for determining polyp versus BVN flow was set by a distance of the average thickness of outer retina (180 µm) in healthy eyes above the Bruch's membrane, with flow located anterior to this cutoff identified as polyp flow and flow posterior as BVN.^{21,22} Our study classified polyps into three categories:

- 1) Type 1: Polyp structures were clearly visible in green color on en face OCTA images. These polyps also exhibited a clear flow signal in the corresponding cross-sectional scans.

- 2) Type 2: Sub-RPE flow signal was observed under peaked PED on cross-sectional scans corresponding to polyps identified on ICGA but without the presence of green polyp structures on en face OCTA. These polyps could be displayed in the same yellow color as BVN on en face OCTA and difficult to be differentiated from BVN by en face OCTA only.
- 3) Type 3: Polyps were identified on ICGA, but no flow was detected on either en face OCTA or cross-sectional scans.

The same algorithmic approach was applied to typical nAMD group to test if the algorithm could differentiate between PCV and non-PCV neovascularization. The presence of polyps on en face OCTA as identified by the algorithm was compared between PCV and nAMD groups.

Statistical Analysis

To compare various metrics across polyp types (I versus II/III), mixed-effects logistic regression models is used, accounting for whether patient was previously treated or naïve to treatment. Detection of polyps on en face OCTA was compared between two methods: polyp count by the slab-specific projection-resolved (PR) algorithm and manual polyp count without the algorithm. The *P* value was calculated from a McNemar's test.

RESULTS

Twenty-nine eyes from 29 patients with PCV and 30 eyes from 30 patients with typical nAMD were enrolled in the study. Overall, the patients' ages ranged from 58 to 88 years old. Among 29 PCV cases, 13 were treatment naïve, 16 received multiple anti-VEGF therapy, and 6 received additional photodynamic therapy (PDT). Among 30 nAMD cases, 24 cases (80%) were type 1 neovascularization (NV), 5 cases (17%) were type 2 NV, and 1 case (3%) was type 3 NV. ICGA images identified 56 polyps from 29 PCV eyes. The polyps were classified into 3 types by slab-specific PR OCTA algorithm: type 1, 38 polyps (68%) clearly visible in green color on en face OCTA images with clear flow signal in the corresponding cross-sectional scans (Figs. 1, 2); type 2, 13 polyps (23%) not showing a green signal on en face images but showing yellow sub-RPE flow signal under PED on cross-sectional scans corresponding to polyps on ICGA; and type 3, 5 polyps (9%) with no flow on both en face OCTA and cross-sectional scans. Representative cases of the 3 types of polyps are shown in Figure 3. En face OCTA alone were able to detect more polyps using the slab-specific PR algorithm (68%) compared to manual counting on conventional en face OCTA images (30%, *P* = 0.0001; Fig. 4). Combining the en face outer retinal OCTA and cross-sectional OCTA scans increased polyp detection rate to 91% (types 1 and 2 polyps) relative to the gold standard ICGA imaging.

After applying the slab-specific PR algorithm, 83% of the nAMD group demonstrated absence of polyps (absence of

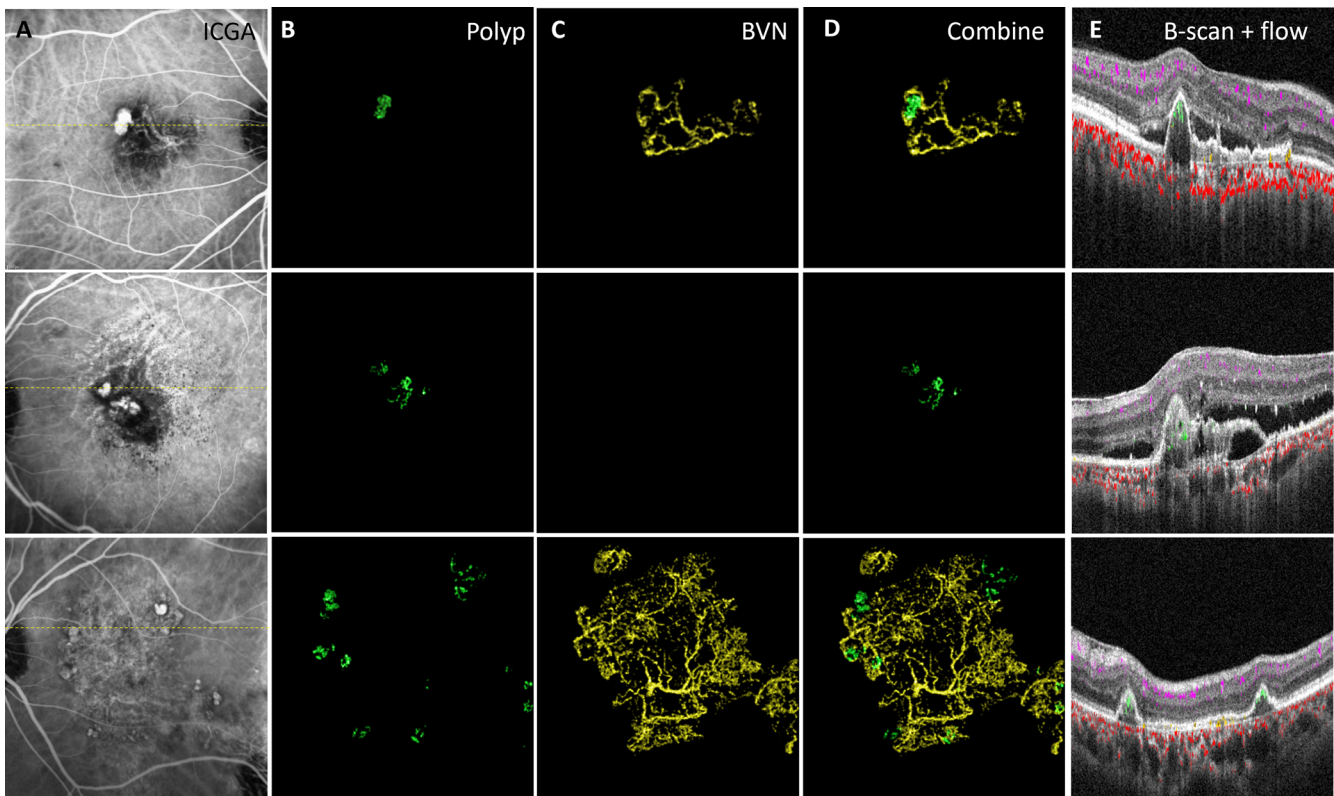


FIGURE 1. Multimodal images from three patients diagnosed with polypoidal choroidal vasculopathy. (A) ICGA images demonstrated bright hypercyanescence polypoidal structures in all 3 patients, with BVN observed in patients 1 (top row) and 3 (bottom row). (B) En face images using slab-specific projection-resolved OCTA algorithm for enhancing polyp detection coded in green color. (C) En face OCTA images display the BVN, coded in yellow, separately from the polyp structures. (D) En face OCTA images combining the area of polyps with BVN. (E) Cross-sectional OCTA images, corresponding to the yellow horizontal dotted line in column A, showing flow overlay in the polyp and BVN.

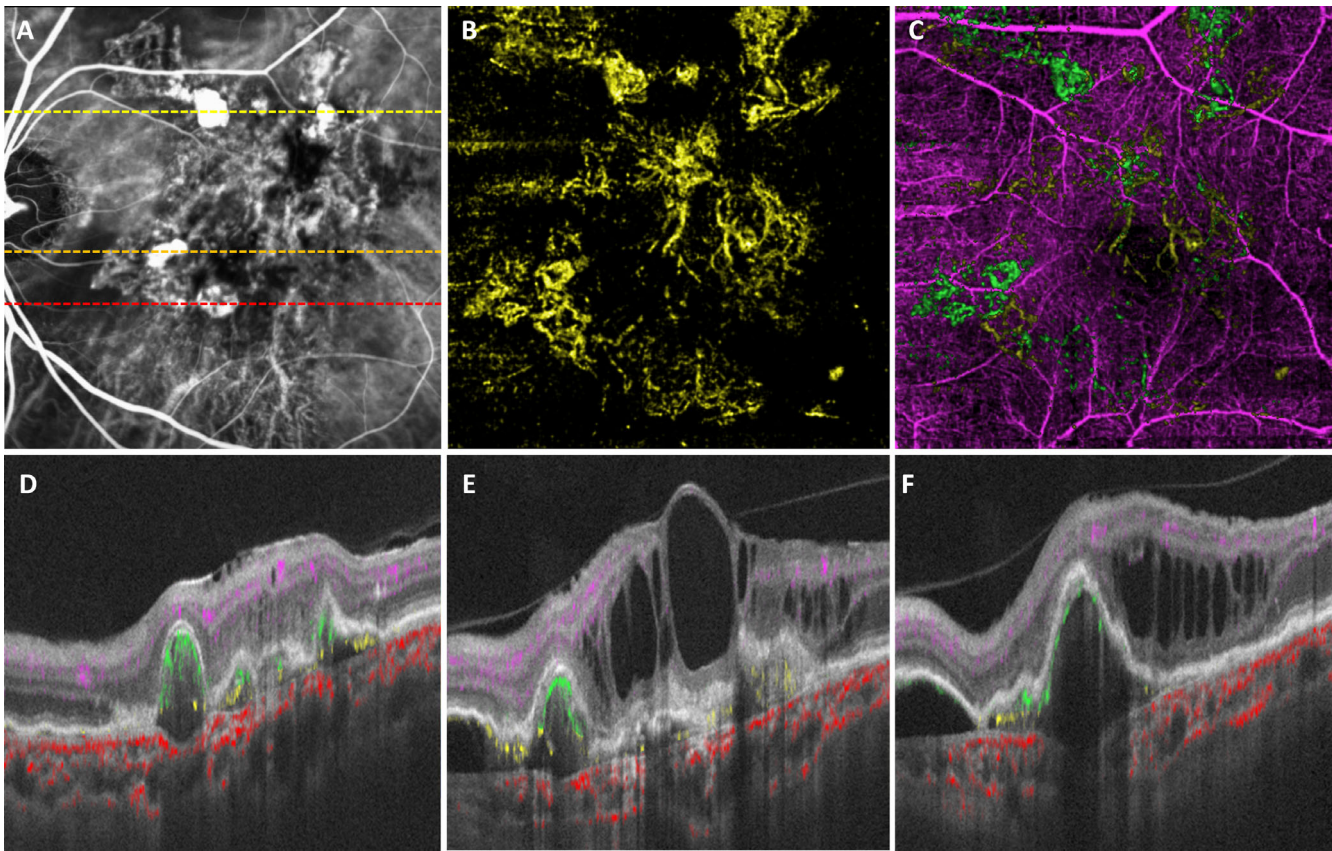


FIGURE 2. Multimodal images of a patient diagnosed with chronic polypoidal choroidal vasculopathy. **(A)** ICGA image clearly demonstrated multiple polyps in the posterior pole. **(B)** En face OCTA without applying the slab-specific projection-resolved algorithm for enhancing polyp detection. **(C)** En face OCTA with the slab-specific projection-resolved algorithm, where polyps are highlighted in green, and BVN is coded in yellow. **(D, E, F)** Cross-sectional OCTA images show flow overlay in the polyp and BVN, corresponding to the yellow, orange, and red horizontal dotted lines in **A**, respectively.

green color) and were correctly classified as typical nAMD. The other 17% of nAMD cases showed falsely detected polyps due to flow signals at the apices of large PEDs (Fig. 5).

Characteristics like PED height (>180 μm) and the presence of luminal structure under the RPE significantly influenced the visualization of polyps as type 1 on en face OCTA by our algorithm. Smaller polyp size and absence of halo appearance on ICGA were predominant in type 2 and type 3 polyps compared to type 1 polyps. No statistically significant difference in polyp filling time on ICGA was observed among the polyp types. The structural OCT revealed fluid or blood components above the RPE in all type 3 polyps, 46.2% in type 2, and 15.8% in type 1 but the difference did not reach significance. The overlying RPE showed atrophic changes in most of the cases, which tends to be more predominant in chronic recurrent cases. Details are summarized in the Table.

In type 2 and type 3 polyps, 82% were treatment naïve, in which 33% were chronic polyps presented for more than 1 year duration without treatment. The other 18% were previously treated by multiple anti-VEGF injections.

It was observed that most of the polyps on cross-sectional OCTA could appear as luminal structures with vascular flow at their borders. Polyp centers were filled with heterogeneous hypo-hyper reflectivity and lacked flow. Interestingly, en face OCTA and corresponding cross-sectional scans of two polyps demonstrated prominent flow at the boundary

of the polyps, contrasting with poorly visualized vascular structure of the polyps on ICGA (Fig. 6).

DISCUSSION

OCTA is a fast and noninvasive tool for detecting macular blood flow. Whereas ICGA remains a gold standard for PCV diagnosis, OCTA has gained in popularity and usability over the past decade. Various groups have explored OCTA's potential in detecting polyps in PCV, with sensitivity ranging from 43.9% to 100% compared to ICGA.^{10–12,16,23–26} Results from most studies rely on both en face and cross-sectional OCTA images. Although grading PCV based on cross-sectional OCTA could show high accuracy, the en face view of neovascularization in PCV has not been fully revealed and characterized. En face OCTA images can provide better visualization and quantitative analysis. When focusing solely on en face OCTA, polyp detection can become challenging. Our results showed a 30% polyp detection rate through manual counting on conventional en face OCTA compared to ICGA. Similar to a study from Cheung et al., who reported only 43.5% sensitivity in detecting polyps by en face OCTA.¹⁶ Reasons for en face OCTA's potential failure in detecting every polyp seen by ICGA include low signal penetration through the heavily pigmented RPE, signal reduction artifact, projection artifact, segmentation errors, slow blood flow

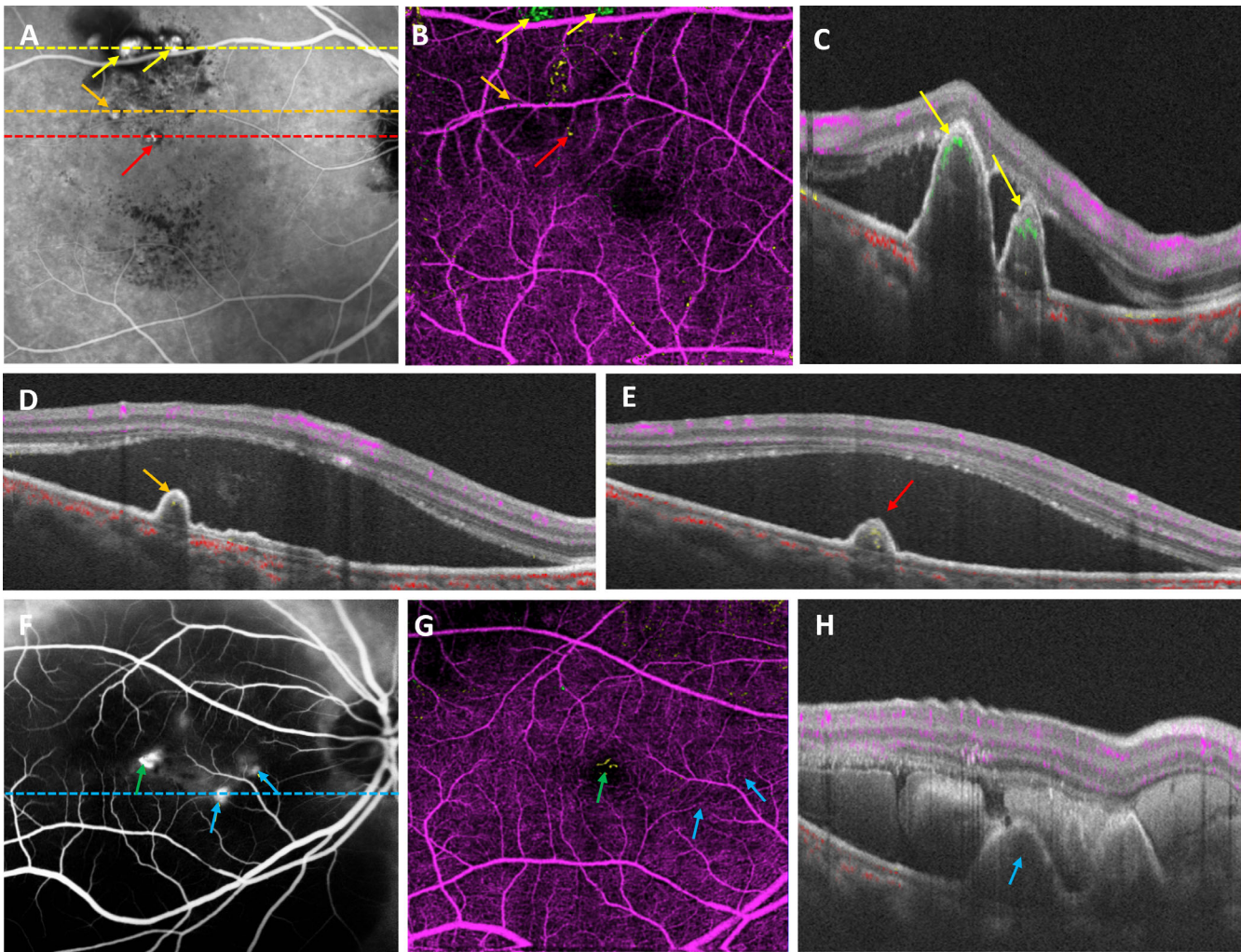


FIGURE 3. Multimodal images from two patients showed three categories of polyps in our study based on their visualization in en face and cross-sectional OCTA. (A) ICGA image from the first patient demonstrated four superior extrafoveal hypercyanescence polyps. (B) En face OCTA with slab-specific projection-resolved algorithm successfully highlights two polyps in *green color* superior to the retinal vessel (type 1 polyps, indicated by the *yellow arrows*), whereas the other two polyps remain undetected (type 2 polyps, marked by *orange* and *red arrows*). (C, D, E) Cross-sectional OCTA images, corresponding to the *yellow*, *orange*, and *red* horizontal dotted lines in A, respectively, show flow overlay in the polyps. (F) An ICGA image from the second patient, who presented with massive subretinal hemorrhage, demonstrates one type 2 polyp in the central fovea (*green arrow*) and two type 3 polyps nasally (*blue arrows*). The type 3 polyps show no flow in both en face OCTA (G) and cross-sectional OCTA (H) at the level of the *blue dotted line* in F.

within polyps, and, most importantly, inherent difficulties in distinguishing polyp flow from adjacent BVN.

Polyps in a recent study and our study exhibited a luminal structure with a prominent flow at the border of the polyp on cross-sectional scans.²⁷ However, on en face images, many polyps demonstrated a tangle or loop of vessels connecting to the distal end of the BVN (see Figs. 2, 6). This concurs with a study by Bo et al., which demonstrated a cluster of tangled vessels associated with the termination of the BVN in polypoidal lesions.²⁸ Teo et al. studied the vascular structure of polyps by 3-dimensional reconstruction with swept-source OCTA (SS-OCTA). They found that polyps appeared as a coil-like, spiraling vasculature which attached to the back of the RPE layer.²⁹ As a result, these vascular features of the polyps contribute to difficulties in distinguishing polyps from BVN on en face OCTA alone, where focal aneurysmal-like dye filling is undetectable as opposed to ICGA.

Both segmentation and projection artifacts can be major sources of error for polyp detection. Segmentation artifacts can incorrectly remove polyp flow, whereas projection artifacts on the strongly reflective RPE can be conflated with polyp flow. This can be problematic, especially for detecting smaller polyps, where the number of flow pixels could be small. Furthermore, because polyp flow occurs in posterior layers, signal attenuation can lead to a reduced signal-to-noise ratio, making flow difficult to recognize. In these circumstances, it is especially important that any flow signal be unambiguously *in situ* in order to correctly catalog the number and characteristics of polyps. To address this issue, our advanced technology of PR-OCTA algorithm is used to enhance the reflectance signal of both polyps and BVN in the outer retina while simultaneously eliminating segmentation and projection artifacts. This enhancement significantly improves the visualization of the flow within polyps and BVN beneath the RPE layer.

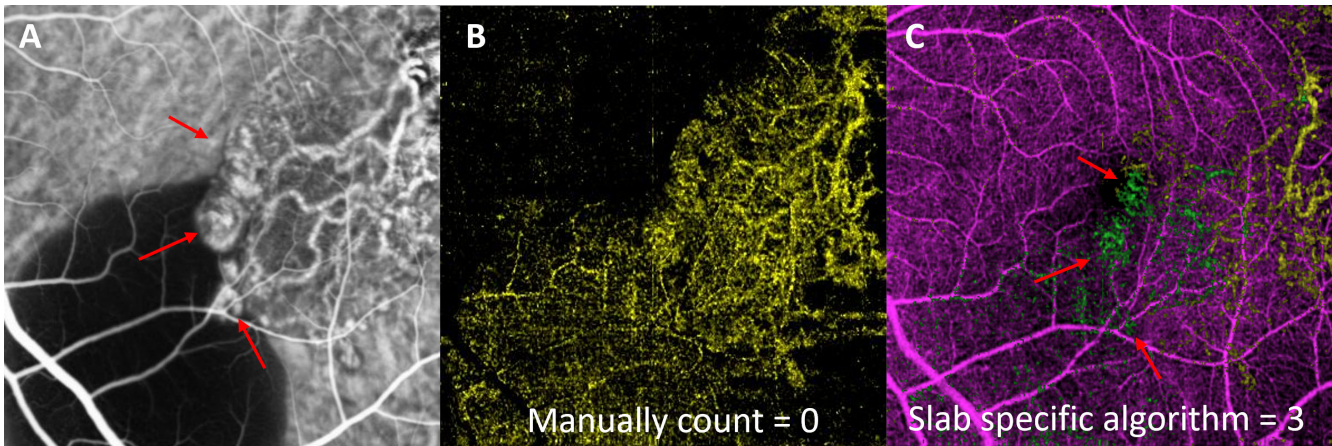


FIGURE 4. Polyp detection on en face OCTA image by manual counting and slab-specific PR algorithm. (A) ICGA images illustrated multiple hypercyanescence foci of the polyps (red arrows). (B) En face OCTA without the slab-specific PR algorithm showing the polyp structures are difficult to be differentiated from adjacent BVN. (C) En face OCTA with the slab-specific PR algorithm facilitated easy detection of polyp locations (coded in green) without cross-sectional OCTA requirement.

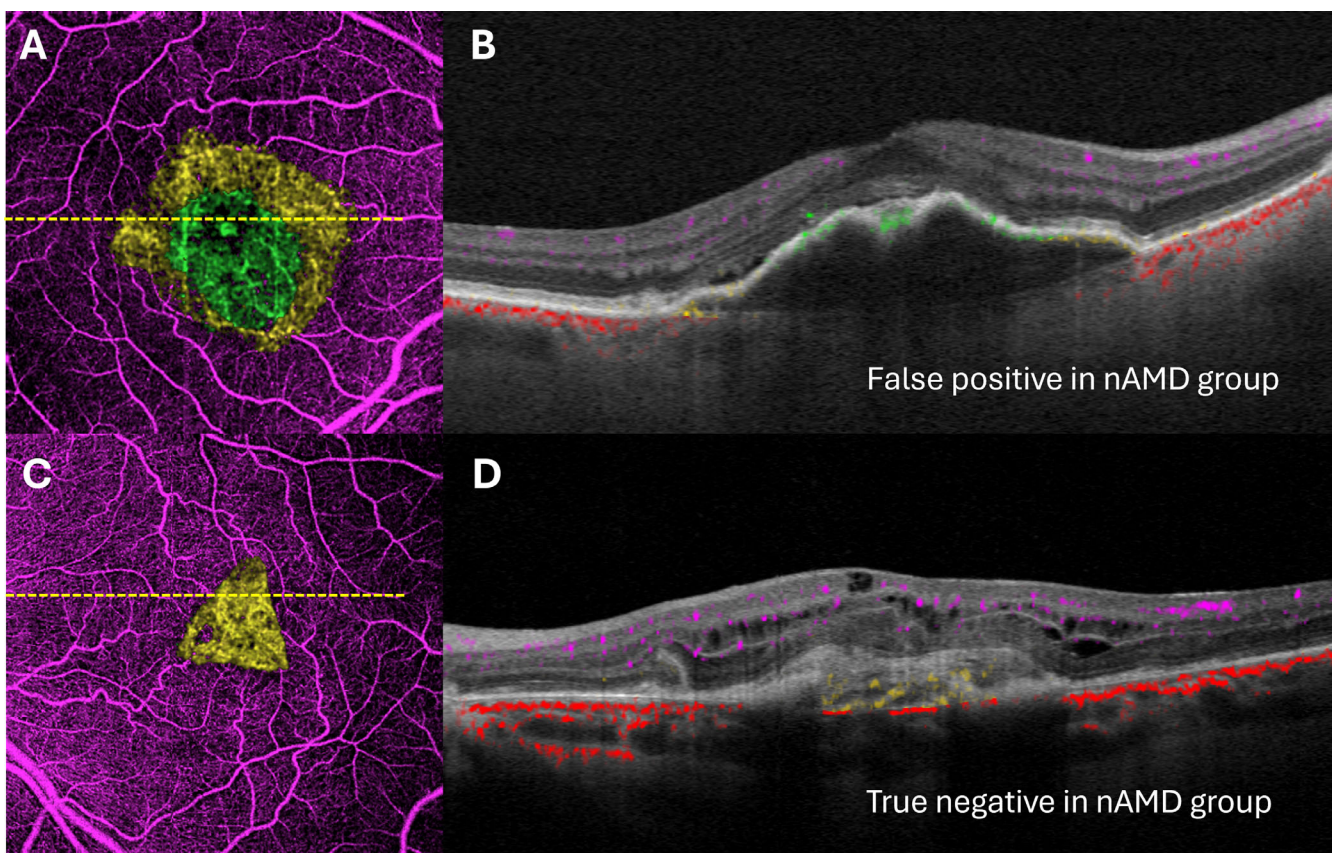


FIGURE 5. En face OCTA and cross-sectional OCTA images reveals false positive (A and B) and true negative (C and D) polypoidal structures in neovascular AMD cases.

In this study, we propose an advanced slab-specific PR-OCTA algorithm for en face polyp detection. Its primary advantage lies in its capability to precisely segment different thickness levels of PEDs and represent them with distinct colors. This facilitates the differentiation of polyp flow within highly elevated PED from BVN flow in less elevated PED. Consequently, polyps can be easily visualized using a single en face OCTA image, compared with

ICGA images. With this approach, we successfully identified two-thirds (68%) of polyps using just the en face OCTA images (see Figs. 1, 2) compared with a 30% polyp detection rate without applying the algorithm. This emphasizes the algorithm's advantage in easy utilization in a real clinical setting. Most of these type 1 polyps exhibited common characteristics, such as a prominent luminal structure beneath the RPE, high PED height, greater polyp size,

TABLE. Characteristics of SD-OCT and ICGA Findings Associated With Flow Detection on En Face OCTA With our Algorithm

Number of Polyps	Visualized Polyps (Type 1 Polyps) <i>N</i> = 38		Non-Visualized Polyps (Type 2 and 3 Polyps) <i>N</i> = 18		<i>P</i> Value*
SD-OCT characteristics					
Fluid/blood component above polyp	6 (15.8%)		11 (61.1%)		0.109
Atrophic RPE above polyp	28 (73.7%)		15 (83.3%)		0.731
Luminal structure under RPE	21 (55.3%)		2 (11.1%)		0.011
Heterogeneous content in PED	38 (100%)		17 (94.4%)		0.99
PED height at polyp location, um	<180	11 (28.9%)	12 (66.7%)		0.001
	>180	27 (71.1%)	6 (33.3%)		
ICGA characteristics					
Time first seen polyp, s					
Median [min, max]	24.0 [15.0, 32.0]		21.0 [14.0, 74.0]		
Mean (SD)	23.1 (3.81)		23.7 (5.08)		0.936
Time to complete fill polyp in ICGA					
<1 min	21 (72%)		13 (72%)		0.522
1–2 min	6 (24%)		2 (11%)		
>2 min	1 (3.4%)		3 (17%)		
Mean size polyp in ICGA, mm ² (SD)	0.182 (0.171)		0.0722 (0.039)		0.024
Halo around polyp	22 (57.9%)		8 (44.4%)		0.001
Polyp leakage	2 (5.3%)		6 (33.3%)		0.193
Pulsatile polyp	3 (7.9%)		3 (16.7%)		0.657
Polyp wash out in late phase	14 (36.8%)		11 (61.1%)		0.299

* *P* value from mixed-effects logistic regression models, accounting for whether patient was previously treated or naïve to treatment.

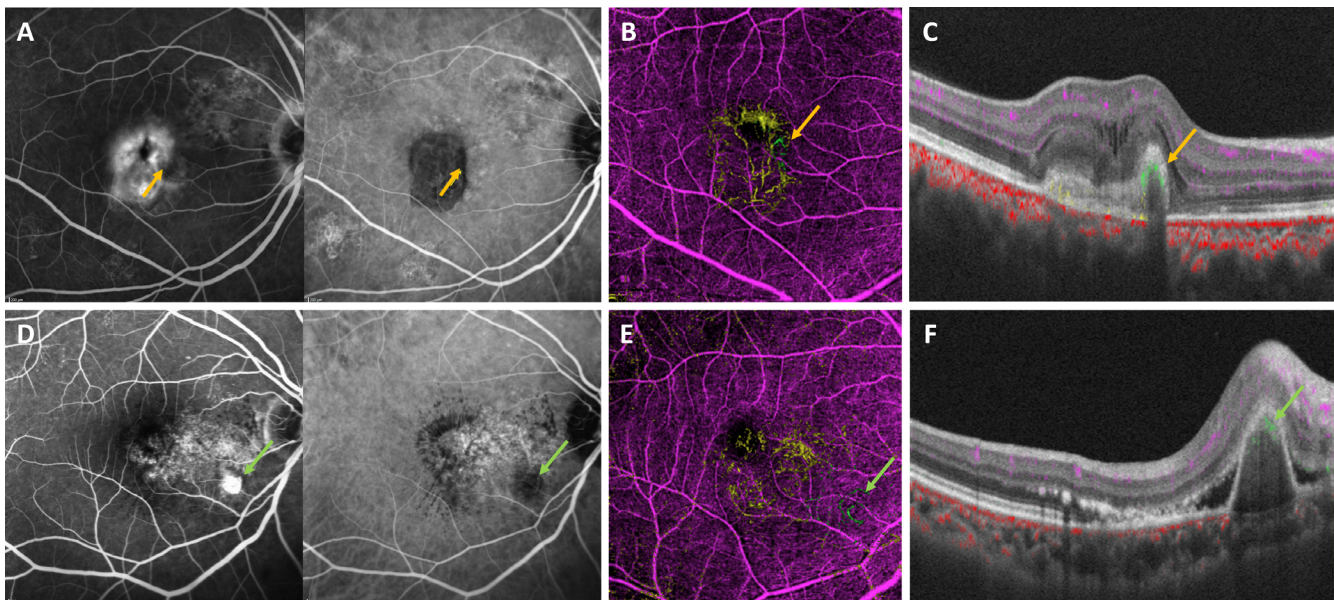


FIGURE 6. En face OCTA reveals polyp structures in two cases with poor visualization of polyps in ICGA images. **(A, D)** Simultaneous FFA and ICGA images demonstrated faint hypercyanescence areas of the polyps (yellow and green arrows). **(B, E)** En face OCTA with the slab-specific projection-resolved algorithm could detect blood flow (coded in green) within the polyps. **(C, F)** Cross-sectional OCTA images clearly show flow overlay within both polyps.

and presence of a halo around the polyp structure on ICGA (see the Table).

Because the algorithm was developed based on the characteristic OCT anatomy of the PCV lesions, it has potential to differentiate between PCV and typical nAMD which has different morphological features by en face OCTA. The clinical applicability of our algorithm was further explored by running the algorithm on OCTA images of patients with typical nAMD (non-PCV) to differentiate PCV and non-PCV macular neovascularization. The accuracy of not detecting polyps in patients with nAMD was 83%. A false positive

rate of detecting polyp was 17% in nAMD cases resulting from high PED height. However, the appearance of the polyp structure was not observed as a focal round shape structure (see Fig. 5). This relatively high accuracy of differentiating PCV and non-PCV macular neovascularization suggests that our approach is clinically adaptable and warrants further refinement to improve its accuracy.

Type 2 polyps were the polyps underneath low-lying PED. They were difficult to be distinguished from BVN signals using en face OCTA alone. They were less likely to demonstrate luminal structures on OCT and tended to be

smaller in size compared to type 1 polyps. This might reflect a small size or partial regression of the polyps and the flow inside these polyps might be at a similar speed as the BVN.

Approximately 9% of the polyps in our study did not exhibit flow on both en face and cross-sectional OCTA (see Figs. 3F–H). Most of these type 3 polyps were of smaller size or might be obscured by blood or fluid above the RPE or between the RPE and the polyps. When a massive hemorrhage was observed, OCTA was not effective in polyp detection.

Previous studies reported several factors related to the visibility of polyps on OCTA including the choroid-to-polyp dye filling time on ICGA³⁰ and the presence of pulsating polyps in ICGA.¹⁰ Our study also looked for these factors but failed to demonstrate significant association with the polyp visibility on en face OCTA using our algorithm. Unlike our study, Zhan et al. observed the greater height of polyp was associated with non-visualized polyp on OCTA.³¹ These differences could be explained by our advanced PR-OCTA algorithm that segmented and enhanced *in situ* flow.

ICGA has long been considered the gold standard for PCV diagnosis. However, with the advancement of technology in OCTA, comparable results in identifying polyps have been demonstrated.³² Two cases from our study highlighted the greater potential of OCTA in visualizing vascular flow in en face and cross-sectional OCTA images, particularly in cases where faint hypercyanescence polyps were observed in ICGA (see Fig. 6). OCTA may be more sensitive than ICGA in detecting polyps with subtle activity in certain cases.

Our novel slab-specific PR-OCTA algorithm offers several advances compared with standard OCTA. First, it removes the ambiguity of projection artifacts and reveals all *in situ* flow through the entire OCTA volume. Second, a slab-specific strategy can help to differentiate pathologic flow based on their locations (relative to the heights of PEDs). This method requires the segmentation from Bruch's membrane only (which is a relatively easy segmentation, frequently available on commercial devices). This minimal segmentation requirement allows the method to be more practical and clinically adaptable. Our study shows this strategy has been quite effective and straightforward in highlighting polyp structures (in green) from adjacent BVN areas (in yellow) accurately. Its accuracy in differentiating PCV and non-PCV macular neovascularization is relatively high. Taken together, slab-specific PR-OCTA is a fast, easy, and efficient tool for detecting PCV in clinical settings using a single instrument. It would facilitate not only PCV diagnosis but also repeated evaluation of treatment responses and patients' education in clinics. Using swept-source, a fast wavelength scanning light source, could also further improve the polyp detection rate in the future.

Limitations of this study include a limited number of subjects and variations in disease stages, leading to diverse polyp characteristics that could affect the polyp detection rate. The chronicity of PCV can influence polyp size, activity, or degree of RPE atrophy overlying polyp, which affects its visualization on en face OCTA. However, our objective was to compare the polyp detection rate between ICGA and our slab-specific projection-resolved en face OCTA regardless of chronicity of the lesions. Steep PEDs can cause segmentation errors and manual corrections were still required in some instances. These segmentation errors can be mitigated in the future by improving our AI-based segmentation algorithms. Despite the significantly improved sensitivity shown by our algorithm, certain polyps were occasionally missed due to

their small size, low height, or indistinctive features. In a minority of typical nAMD cases, large PEDs could give false positive results for PCV by our algorithm. A future study with a larger sample size along with AI-based approaches would be useful to further improve the novel slab-specific PR algorithm of this study.

CONCLUSIONS

OCTA, with advanced algorithmic support for slab segmentation and projection artifact removal, could improve the en face detection of flow in polyps. By using our slab-specific PR algorithm, the polyp detection rate from en face OCTA improved from only 30% to 68% in this study. The accuracy of differentiating PCV from typical nAMD was 83%. It is a fast, easy, and efficient tool for detecting PCV in clinical settings using a single instrument and without the risk of dye injection. According to our algorithm, the absence of a luminal structure on OCT at the polyp site, small polyp size, and the absence of a halo on ICGA were associated with a reduced polyp detection rate on en face OCTA.

Acknowledgments

Supported by the National Institute of Health (R01 EY035410, R01 EY027833, R01 EY024544, R01 EY031394, R01 EY023285, T32 EY023211, UL1TR002369, and P30 EY010572); the Malcolm M. Marquis, MD Endowed Fund for Innovation; an Unrestricted Departmental Funding Grant and H. James and Carole Free Catalyst Award from Research to Prevent Blindness (New York, NY), Edward N. & Della L. Thome Memorial Foundation Award, and the Bright Focus Foundation (G2020168 and M20230081).

Oregon Health & Science University (OHSU), Yali Jia, and Jie Wang have a significant financial interest in Optovue/Visionix, Inc. and Genentech, Inc.; OHSU and Yali Jia also have a significant financial interest in Optos, Inc. These potential conflicts of interest have been reviewed and managed by OHSU.

Disclosure: **N. Wongchaisuwat**, None; **J. Wang**, Optovue/Visionix Inc. (P, R), Roche/Genentech, Inc. (P, R); **T.T. Hormel**, None; **Y. Jia**, Optovue/Visionix, Inc. (P, R), Roche/Genentech, Inc. (P, R, F), Optos, Inc. (P); **E.S. White**, None; **N. Rodanant**, None; **N. Phasukkijwatana**, None

References

1. Balaratnasingam C, Lee WK, Koizumi H, Dansingani K, Inoue M, Freund KB. Polypoidal choroidal vasculopathy: a distinct disease or manifestation of many? *Retina*. 2016;36(1):1–8.
2. Teo KYC, Cheung GCM. New concepts in polypoidal choroidal vasculopathy imaging: a focus on optical coherence tomography and optical coherence tomography angiography. *Asia Pac J Ophthalmol (Phila)*. 2019;8:165–171.
3. Cheung CMG, Lai TYY, Ruamviboonsuk P, et al. Polypoidal choroidal vasculopathy: definition, pathogenesis, diagnosis, and management. *Ophthalmology*. 2018;125(5):708–724.
4. Bhoomibunchoo C, Yospaiboon Y, Thoongsuwan S, et al. Idiopathic polypoidal choroidal vasculopathy in Thai patients with clinical and angiographic choroidal neovascularization. *Clin Ophthalmol*. 2017;11:317–322.
5. Lorentzen TD, Subhi Y, Sørensen TL. Prevalence of polypoidal choroidal vasculopathy in white patients with exudative age-related macular degeneration: systematic review and meta-analysis. *Retina*. 2018;38(12):2363–2371.

6. Spaide RF, Fujimoto JG, Waheed NK. Optical coherence tomography angiography. *Retina*. 2015;35(11):2161–2162.
7. Spaide RF, Fujimoto JG, Waheed NK, Sadda SR, Staurenghi G. Optical coherence tomography angiography. *Prog Retin Eye Res*. 2018;64:1–55.
8. Jia Y, Bailey ST, Hwang TS, et al. Quantitative optical coherence tomography angiography of vascular abnormalities in the living human eye. *Proc Natl Acad Sci USA*. 2015;112(18):E2395–E2402.
9. Campbell JP, Zhang M, Hwang TS, et al. Detailed vascular anatomy of the human retina by projection-resolved optical coherence tomography angiography. *Sci Rep*. 2017;7:42201.
10. Tanaka K, Mori R, Kawamura A, Nakashizuka H, Wakatsuki Y, Yuzawa M. Comparison of OCT angiography and indocyanine green angiographic findings with subtypes of polypoidal choroidal vasculopathy. *Br J Ophthalmol*. 2017;101(1):51–55.
11. Wang M, Zhou Y, Gao SS, et al. Evaluating polypoidal choroidal vasculopathy with optical coherence tomography angiography. *Invest Ophthalmol Vis Sci*. 2016;57(9):Oct526–Oct532.
12. Tomiyasu T, Nozaki M, Yoshida M, Ogura Y. Characteristics of polypoidal choroidal vasculopathy evaluated by optical coherence tomography angiography. *Invest Ophthalmol Vis Sci*. 2016;57(9):Oct324–Oct330.
13. Jia Y, Tan O, Tokayer J, et al. Split-spectrum amplitude-decorrelation angiography with optical coherence tomography. *Opt Express*. 2012;20(4):4710–4725.
14. Choi W, Moult EM, Waheed NK, et al. Ultrahigh-speed, swept-source optical coherence tomography angiography in nonexudative age-related macular degeneration with geographic atrophy. *Ophthalmology*. 2015;122(12):2532–2544.
15. Rebhun CB, Moult EM, Novais EA, et al. Polypoidal choroidal vasculopathy on swept-source optical coherence tomography angiography with variable interscan time analysis. *Transl Vis Sci Technol*. 2017;6(6):4.
16. Cheung CMG, Yanagi Y, Akiba M, et al. Improved detection and diagnosis of polypoidal choroidal vasculopathy using a combination of optical coherence tomography and optical coherence tomography angiography. *Retina*. 2019;39(9):1655–1663.
17. Koh A, Lee WK, Chen IJ, et al. EVEREST study: efficacy and safety of verteporfin photodynamic therapy in combination with ranibizumab or alone versus ranibizumab monotherapy in patients with symptomatic macular polypoidal choroidal vasculopathy. *Retina*. 2012;32(8):1453–1464.
18. Guo Y, Camino A, Zhang M, et al. Automated segmentation of retinal layer boundaries and capillary plexuses in wide-field optical coherence tomographic angiography. *Biomed Opt Express*. 2018;9(9):4429–4442.
19. Wang J, Zhang M, Hwang TS, et al. Reflectance-based projection-resolved optical coherence tomography angiography [Invited]. *Biomed Opt Express*. 2017;8(3):1536–1548.
20. Wang J, Hormel TT, Bailey ST, Hwang TS, Huang D, Jia Y. Signal attenuation-compensated projection-resolved OCT angiography. *Biomed Opt Express*. 2023;14(5):2040–2054.
21. Arepalli S, Srivastava SK, Hu M, et al. Assessment of inner and outer retinal layer metrics on the Cirrus HD-OCT Platform in normal eyes. *PLoS One*. 2018;13(10):e0203324.
22. Shao L, Zhang QL, Zhang C, et al. Thickness of retinal pigment epithelium - Bruch's membrane complex in adult Chinese using optical coherence tomography. *Eye (Lond)*. 2023;37(1):155–159.
23. de Carlo TE, Kokame GT, Shantha JG, Lai JC, Wee R. Spectral-domain optical coherence tomography angiography for the diagnosis and evaluation of polypoidal choroidal vasculopathy. *Ophthalmologica*. 2018;239(2–3):103–109.
24. Huang CH, Yeh PT, Hsieh YT, Ho TC, Yang CM, Yang CH. Characterizing branching vascular network morphology in polypoidal choroidal vasculopathy by optical coherence tomography angiography. *Sci Rep*. 2019;9(1):595.
25. Wang Y, Yang J, Li B, Yuan M, Chen Y. Detection rate and diagnostic value of optical coherence tomography angiography in the diagnosis of polypoidal choroidal vasculopathy: a systematic review and meta-analysis. *J Ophthalmol*. 2019;2019:6837601.
26. de Carlo TE, Kokame GT, Kaneko KN, Lian R, Lai JC, Wee R. Sensitivity and specificity of detecting polypoidal choroidal vasculopathy with en face optical coherence tomography and optical coherence tomography angiography. *Retina*. 2019;39(7):1343–1352.
27. Fujita A, Kataoka K, Takeuchi J, et al. Diagnostic characteristics of polypoidal choroidal vasculopathy based on b-scan swept-source optical coherence tomography angiography and its interrater agreement compared with indocyanine green angiography. *Retina*. 2020;40(12):2296–2303.
28. Bo Q, Yan Q, Shen M, et al. Appearance of polypoidal lesions in patients with polypoidal choroidal vasculopathy using swept-source optical coherence tomographic angiography. *JAMA Ophthalmol*. 2019;137(6):642–650.
29. Teo KYC, Zhao JZ, Klose G, Lee WK, Cheung CMG. Polypoidal choroidal vasculopathy: evaluation based on 3-dimensional reconstruction of OCT angiography. *Ophthalmol Retina*. 2024;8(2):98–107.
30. Fukuyama H, Iwami H, Araki T, Ishikawa H, Ikeda N, Gomi F. Indocyanine green dye filling time for polypoidal lesions in polypoidal choroidal vasculopathy affects the visibility of the lesions on OCT angiography. *Ophthalmol Retina*. 2018;2(8):803–807.
31. Zhan Z, Sun L, Jin C, et al. Comparison between non-visualized polyps and visualized polyps on optical coherence tomography angiography in polypoidal choroidal vasculopathy. *Graefes Arch Clin Exp Ophthalmol*. 2019;257(11):2349–2356.
32. Kim K, Yang J, Feuer W, et al. A comparison study of polypoidal choroidal vasculopathy imaged with indocyanine green angiography and swept-source optical coherence tomography angiography. *Am J Ophthalmol*. 2020;217:240–251.